ADVANCED FUNCTIONAL MATERIALS

Supporting Information

Ultralow Thermal Conductivity of Single-Crystalline Porous Silicon Nanowires

Yunshan Zhao, Lina Yang, Lingyu Kong, Mui Hoon Nai, Dan Liu, Jing Wu, Yi Liu, Sing Yang Chiam, Wai Kin Chim, Chwee Teck Lim, Baowen Li,* John T. L. Thong,* and Kedar Hippalgaonkar*

Supporting Information

Low thermal conductivity of single-crystalline porous Silicon nanowires

Yunshan Zhao[1], Lina Yang[2], Lingyu Kong[1,3], Mui Hoon Nai[4], Dan Liu[1,3], Jing Wu[5], Yi Liu[1], Sing Yang Chiam[5],Wai Kin Chim[1], Chwee Teck Lim[4,6], Baowen Li[7,]*, John T L Thong[1,]*, Kedar Hippalgaonkar[5,]*

[1] Department of Electrical and Computer Engineering, National University of Singapore, Singapore 117583, Republic of Singapore

[2] Department of Mechanical Engineering, California Institute of Technology, Pasadena, California 91125, USA

[3] Graduate School for Integrative Sciences and Engineering, National University of Singapore, Singapore 117456, Republic of Singapore

[4] Mechanobiology Institute, National University of Singapore, Singapore 117411, Republic of Singapore

[5] Institute of Materials Research and Engineering, Agency for Science Technology and Research, Singapore, 117602, Republic of Singapore

[6] Department of Biomedical Engineering, National University of Singapore, Singapore 117576, Republic of Singapore

[7] Department of Mechanical Engineering, University of Colorado, Boulder 80309, USA

S1. Fabrication of porous silicon nanowires

Porous silicon (Si) nanowires were fabricated by metal assisted chemical etching[1, 2] (MacEtch) using a highly doped p-type silicon (100) wafer with resistivity ~ 0.005 Ω.cm, that was cleaved into square pieces, with an area of 1 x 1 cm^2. The samples were pre-cleaned in acetone and isopropyl alcohol (IPA) for a duration of 15 mins each in an ultrasonic bath before removal of the native oxide in dilute 2% hydrofluoric acid (HF). Subsequently, a regular ordered photoresist (S1805) nano-dot array with diameter of ~300 nm and period of ~900 nm was patterned by laser interference lithography. 20 nm Au was evaporated on the Si substrate by a Denton electron beam evaporator with deposition rate at 0.5 Å/s. Since the ratio of metal thickness and nanodot height (~400nm) is very small, a subsequent lift-off process is not necessary. Catalytic etching was conducted under yellow light environment in a solution consisting of constant 13.5 M HF, while the molar concentration of H_2O_2 was varied from 0.16 M to 3.4 M. The etched samples were finally rinsed in IPA and methanol before drying on a hot plate at 45 °C. The fabricated substrate is shown in Figure S1 (a) and inset is a 90° tilted view.

The MacEtched Si nanowires were characterized by high-resolution transmission electron microscope (HRTEM). Here, the samples were prepared by sonication of the etched samples in ethanol for 1 minute. The nanowires were then suspended in ethanol and transferred to a TEM copper grid by a glass pipette. After marking the location of crystalline porous silicon nanowires, the grid was transferred to SEM for pick-up of individual nanowires by a nanomanipulator, as shown in Figure S1 (b).
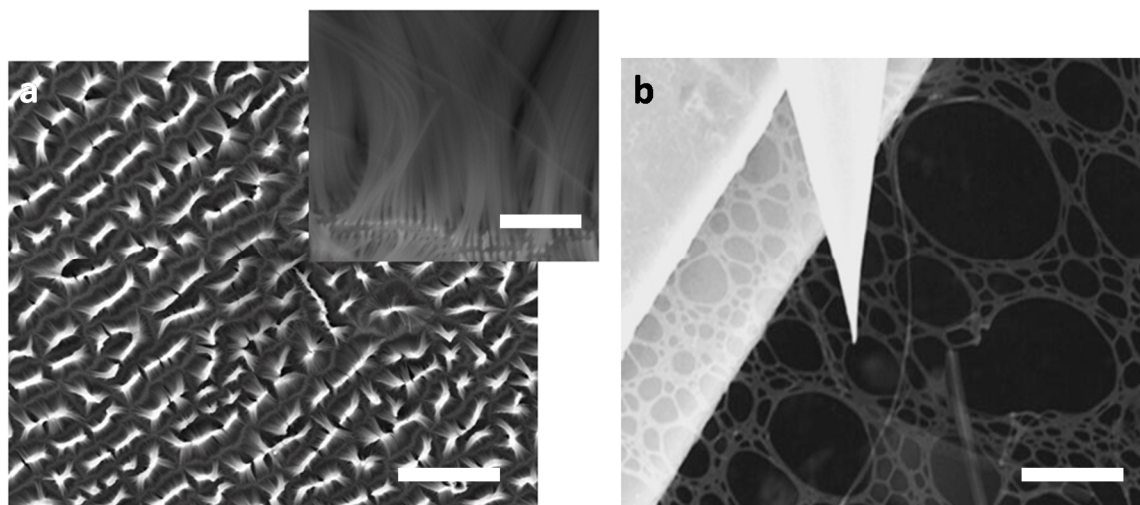
Figure S1. (a) The etched porous silicon nanowires from top view in SEM. Inset is the high magnification image from 90° tilted view. (b) The manipulator tip on top of a TEM copper grid, where a crystalline porous silicon nanowire is located. The scale bars of figure (a), inset and (b) are 100μm, 10μm and 5μm, respectively.
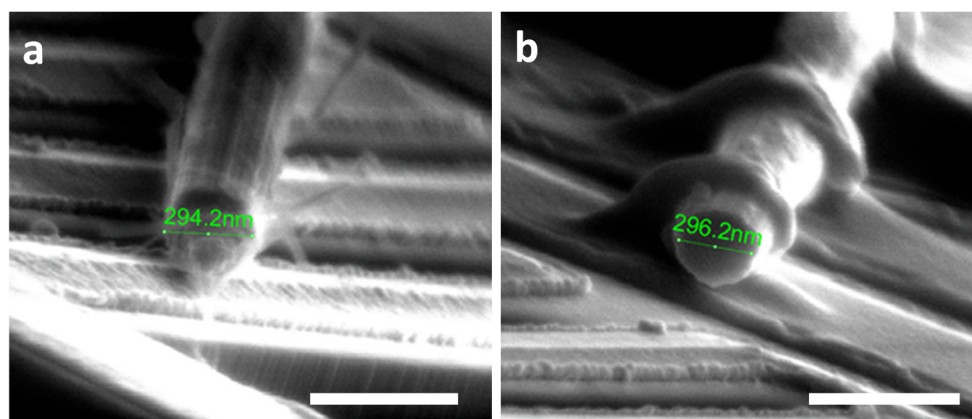

Figure S2. The apparent diameter at the two ends of a porous silicon nanowire shows a uniform diameter across the measured length. The scale bar for (a) and (b) is 500nm.

S2. Structure size calculation and effective thermal conductivity fitting

To measure the structural size of porous silicon nanowires, HRTEM imaging for all the measured nanowires were carried out. As shown in Figure S3 (a)-(c), crystalline lattice fringes surrounding the pore are evident and this crystallinity is maintained throughout the length of the nanowire. The pore boundary is marked using dashed red line and the spacing distribution is shown in Figure S3 (d). Thus, we take the average distance of the structural size as 4.3 ±1.5 nm.

For comparison, we summarize the thermal conductivity of different porous silicon nanostructures in Table S1, including the data in this work and other people's work. Holey silicon[3], porous silicon[4] and phononic nanomesh[5, 6] are taken for comparison. The effective fitting is obtained by multiplying the measured thermal conductivity by the renormalized group velocity given by $v_{eff} = v(1 - P)$, and hence $\kappa_{eff} > \kappa_{measured}$ as seen in columns 1 and 5 in Table S1.
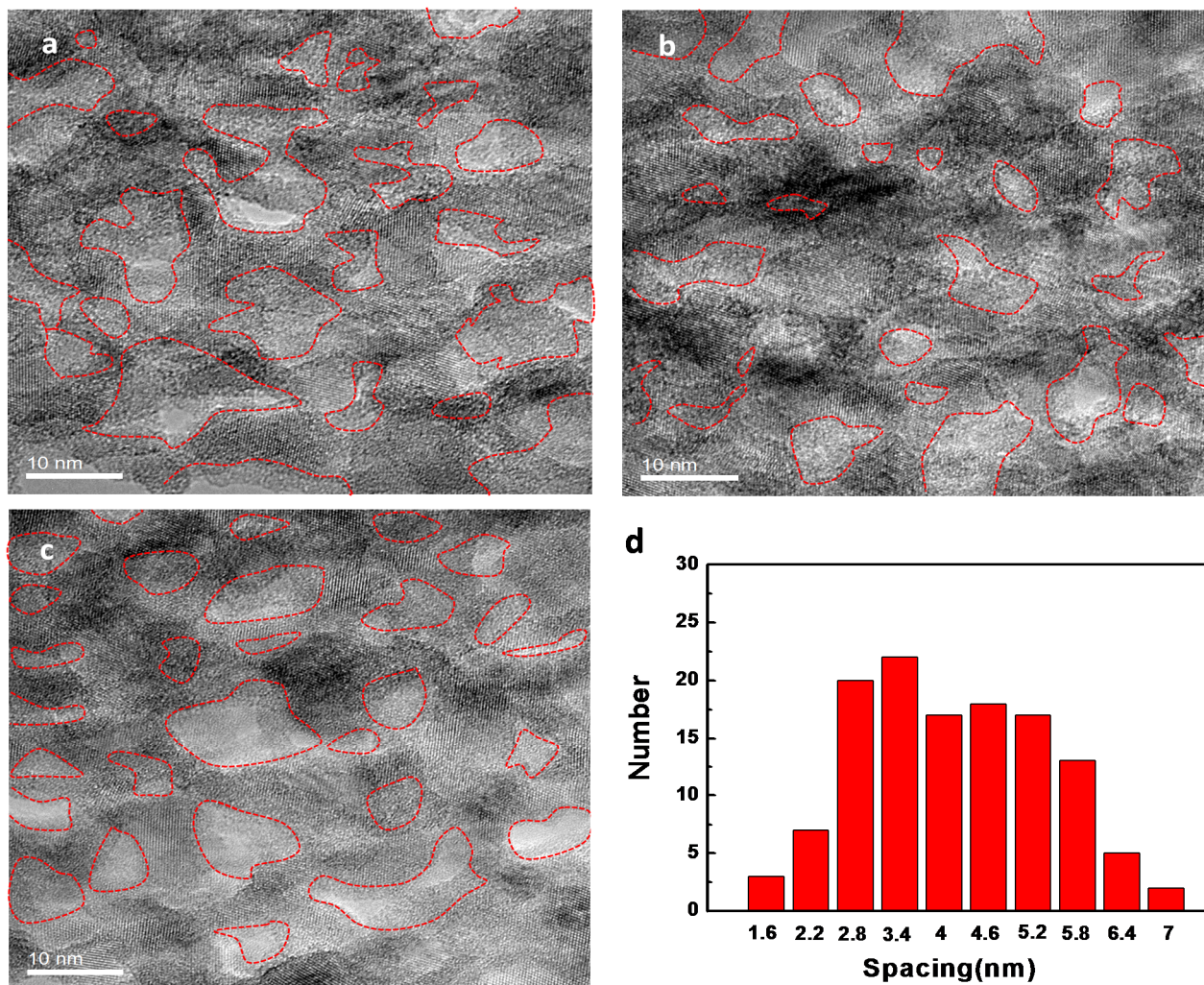
Figure S3. (a), (b) and (c) show HRTEM of porous silicon nanowires. Red dashed line is the pore boundary. The scale bar is shown in each graph. (d) is the histogram of all the structure size spacing in (a), (b) and (c), which is the average distance from edge to edge of pore boundary.

Table S1. Room temperature thermal conductivity of porous silicon nanostructures.

Type of sample	Measured κ (W/mK)	Structure size (nm)	Porosity	κ from Majumdar model (W/mK)	Effective fitting κ (W/mK)
Holey silicon	1.73	23	0.35	9.29	4.13
	6.96	59	0.35	21.78	14.45
	10.23	152	0.35	47.35	22.30
Porous silicon	4.6	8.3	0.38	3.42	8.69
	0.9	7.2	0.62	3.02	3.12
	0.3	7	0.74	2.93	1.34
Phononic nanomesh	41.65	196	0.29	55.98	57
	49.41	304	0.19	71.49	82.04
	80.14	491	0.07	92.7	91.85
	64.54	405	0.14	84.58	86.1
	38.02	275	0.29	68.34	77.48
	76.12	509	0.1	93.21	87.93
	65.39	442	0.16	89.42	86.3
	45.2	367	0.27	79.21	78.71
Phononic nanomesh	1.8	34	0.17	13.11	2.71

S3. Theoretical and experimental verification of absorption power law

Theory:

Due to the Coulomb interaction between the primary electrons penetrating the nanowire and the positive charge of the atomic nucleus, the incident electrons are elastically scattered by the nucleus, causing the electrons to travel diffusively across the nanowire cross-section[7]. In this process, very little energy (less than 1eV) is transferred from the electrons to the specimen. On the other hand, inelastic interactions happen when incident electrons interact with both the tightly bound inner-shell electrons and the loosely bound

outer-shell electrons of the specimen. During this process, a significant portion of the energy of the primary electron, ranging from a fraction of an electron volt to many kilo-electron volts, transfers to the specimen. The scattered angle for inelastic scattering is typically small, of the order of 0.1° or less. To describe the trajectory of incident electrons, Bethe deduced the stopping power equation (modified by Bethe and Ashkin) in the form of $\frac{dE_i}{ds}\left(\frac{KeV}{cm}\right) = 2\pi e^4 N_o \frac{Z\rho}{AE_i} \ln(\frac{1.166E_i}{J})$, $J(KeV) = (9.67Z + 58.5Z^{-0.19}) \times 10^{-3}$ for $Z \geq 13$, where J was the average energy lost per event (keV), ρ the density (g/cm³), Z the atomic number, E_i the electron energy at any point in the specimen (keV), N_o is Avogadro's number, and A the atomic weight (g/mole)[8]. The atomic number, atomic weight and density of silicon are known, which implies that the right side in the above formula is a constant.

The power absorbed by the silicon nanowires (E_i) when irradiated by an electron beam has a linear relation with the electron travelling route (S), thus $E_i = A \bullet S_{solid}(\theta) + B$, where A and B are constants. An illustration of the electron beam travelling through the nanowire cross-section is shown in the schematic of Figure S4. Considering the boundary condition that when $S_{solid}(\theta)$ is 0, the absorption power, E_i would go to 0, we then obtain

$$E_i = A \times S_{solid}(\theta) \qquad\qquad\qquad S(1)$$

From the schematic of Figure S4, the length travelled by each electron at any angle θ is given by:

$$S_{solid}(\theta) = 2 \times \frac{D}{2} \times \frac{\cos(\theta) + \cos(\theta + d\theta)}{2} = D\cos(\theta) \qquad\qquad S(2)$$

And the element for integration in the horizontal direction, $dP_{solid}(\theta)$ is then,

$$dP_{solid}(\theta) = \frac{D}{2} \times \sin(\theta + d\theta) - \frac{D}{2} \times \sin(\theta) = \frac{D}{2}\cos(\theta)d(\theta) \qquad \text{S (3)}$$

Thus, combining S (1) – (3) and assuming a unit length along axial direction of silicon nanowires, we obtain (note the additional factor of 2 comes from the 2nd semicircle)

$$E_{tot} = A \times 2 \times \int_{\theta=0}^{\theta=\frac{\pi}{2}} S_{solid}(\theta) \cdot dP_{solid}(\theta) \times 1 = A \times \frac{\pi}{4}D^2 \qquad \text{S (4)}$$

Similarly, the length traveled by each electron in a porous structure is given by:

$$S_{porous}(\theta) = 2 \times (1-P) \cdot \frac{D}{2} \times \frac{\cos(\theta)+\cos(\theta+d\theta)}{2} = (1-P) \cdot D\cos(\theta) \qquad \text{S (5)}$$

where P is the porosity of porous silicon nanowires and is only counted in the estimation of $S_{porous}(\theta)$. The energy absorbed by a porous silicon nanowire (illustrated in Figure S4 (b)) is then obtained as

$$E_{tot} = A \times 2 \times \int_{\theta=0}^{\theta=\frac{\pi}{2}} S_{porous}(\theta) \cdot dP_{solid}(\theta) \times 1 = A \times (1-P) \times \frac{\pi}{4}D^2 \qquad \text{S (6)}$$

In the CASINO® simulation software, Bethe's expression for power stopping of incident electrons is used as the physical model[9], and the incident electron beam energy loss can be calculated. A constant electron beam energy of 18keV and different cross-section areas of solid silicon nanowires with uniform diameters were employed in our simulation. The use of a large energy of 18keV was to ensure the smallest extent of forward electrons scattering within the silicon nanowires. As shown in Figure 3(a) in main text, when the raster-scanned electron beam energy, E_i, is fixed, the loss of the incident electron energy scales with the cross-sectional area of the nanowires, obtained by considering the integrated projected length across all possible traveling paths.

Experiments:

According to Kanaya and Okayama[10], SEM electrons impinging on the specimens have an interaction volume with the depth of R, following an approximate formula of $R = \frac{0.0276AV^{1.67}}{Z^{0.889}\rho}$ (μm), where A is the atomic weight, V the primary beam voltage, ρ the mass density and Z the atomic number. For silicon, the depth of interaction volume is $3\ \mu m$ when the energy of the electron beam is 18keV, ensuring all the travelling electrons transmit linearly through the measured samples.

Solid silicon nanowires with different diameters were picked up by nano-manipulators in SEM and fixed on the calibrated METS devices by Platinum electron-beam induced deposition (EBID) to make good thermal contact, as shown in Figure S5 (a-d). Then the electron beam with an energy of 18keV was scanned along the nanowires and the absorbed power was recorded in Table S2. TEM was employed to ensure that all the solid silicon nanowires were single-crystalline. Figure S5 (e) is a HRTEM image and (f) is its corresponding diffraction pattern.
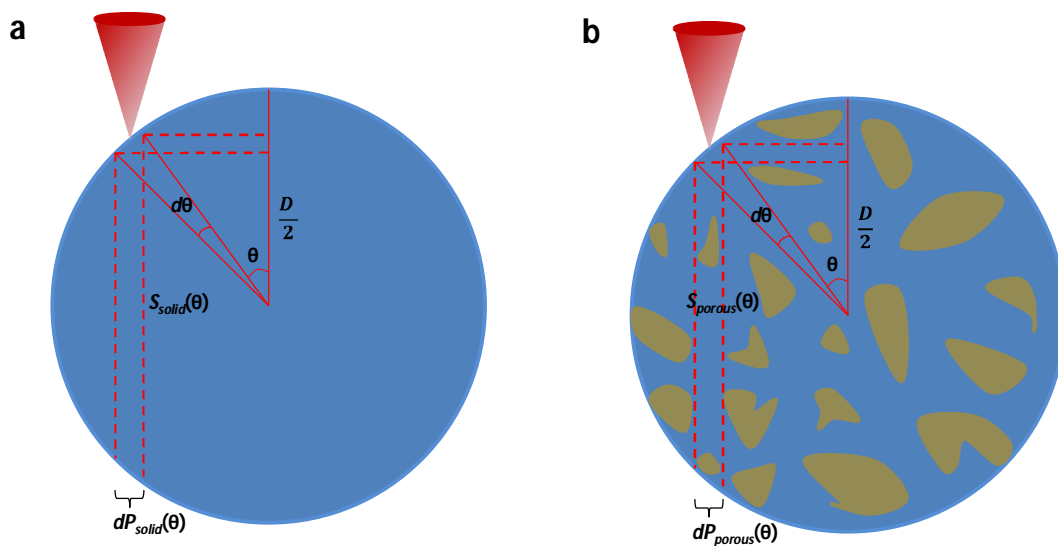
Figure S4. Schematic of a circular cross-section silicon nanowire with the arrow showing the focused electron beam for solid (a) and porous (b) silicon nanowires. $S(\theta)$ and $dP(\theta)$ are the electron traveling trajectory length, and the horizontal element for integration at an angle of θ.
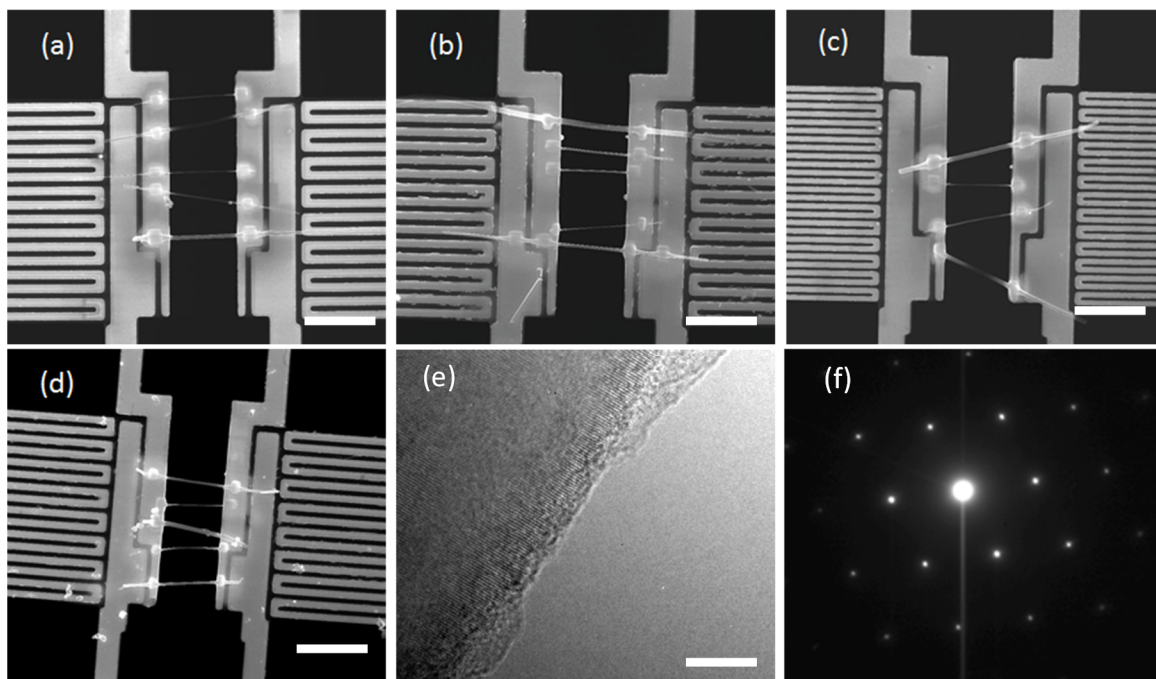
Figure S5. Four devices with different diameter solid silicon nanowires placed on them, where the ends of the nanowires were covered with Platinum using electron beam induced deposition: (a-d). The solid nanowires were characterized by HRTEM (e) and diffraction pattern (f). The scale bars for (a), (b), (c), (d) and (e) are 5 µm, 5 µm, 5 µm, 5 µm and 10 nm, respectively.

Table S2. Experimental verification of power absorption by four devices with different diameter solid silicon nanowires and their absorbed power.

Device	Diameter /nm	Cross-section area /nm^2	Error bar	Absorption power /(nW)	Error bar
1	60.2	2846.31	0.0085	14.93	0.050
	78.4	4827.50	0.032	23.15	0.048
	109.55	9425.72	0.044	37.82	0.070
	240.7	45503.21	0.042	138.50	0.035
2	123.83	12042.22	0.14	35.46	0.031
	87.42	6002.21	0.11	17.91	0.057
	53.5	2248.01	0.067	10.00	0.14
	183.18	26590.44	0.071	90.04	0.039
3	296.05	68302.94	0.051	201.96	0.0091
	70.6	3909.16	0.023	17.92	0.14
	104.35	8027.72	0.018	31.89	0.027
4	174.6	23842.99	0.012	84.92	0.017
	78.55	4845.99	0.079	17.22	0.042
	120.5	11404.18	0.049	39.73	0.063
	191.4	28772.24	0.042	95.68	0.030

S4. Electrical conductivity measurement for Al-doped porous silicon nanowires

The intrinsic electrical conductivity of porous silicon nanowires is quite low, measured as 9.58 (±0.485) $\Omega \cdot m$, according to a four-point probe measurement on at least five samples using a Keithley 4200 (the error bar is from the number of samples measured). Aluminum doping[11] was employed to improve the electrical conductivity. Before annealing the porous silicon nanowires in the furnace, an aluminum film of ~ 8nm thickness was deposited onto the substrate upon which the nanowires are dispersed using a thermal evaporator. The annealing conditions were set at 950℃ for 0.5 hours. After etching away the native oxidation layer by BHF (10:1), the porous silicon nanowires were picked up again onto a METS device. Only the nanowires that were single-crystalline and marked under TEM (with a procedure identical to those described in Methods) were used in this experiment.

Spontaneous formation of an oxidation layer for the porous silicon nanowires is unavoidable when transferring the nanowire to the cryostat, exposed to air even for a few minutes. As shown in Figure S6 (a), two ends of the nanowires were first etched by a Focus Ion Beam (Ga+ ions) with an energy of 30keV, current 10 pA, etching time one second and then deposited immediately by electron beam induced Platinum deposition in the same chamber. The selection of voltage, ion beam current and etching time was carefully calibrated on other nanowires (not used for measurement) to avoid the possibility of amorphization and/or other damage to the nanowires. However, we cannot say with certainty whether the porous crystalline core remains undamaged during this

process. The red dashed square in the insets represents the etched areas by gallium ion beam and the yellow dashed square is the Platinum deposition area. Subsequently, an electrical conductivity of 0.0591 $\Omega \cdot m$ was measured for the nanowire and the same nanowire exhibited a thermal conductivity of 0.48 W/mK at 300K. Therefore, an enhancement of nearly 160 times in the electrical conductivity with a negligible change in the thermal conductivity was observed. Other diffusion-based[12] or ion implantation-based[13] post-doping can be carried out to improve the electrical conductivity further, but this is beyond the scope of our current work.
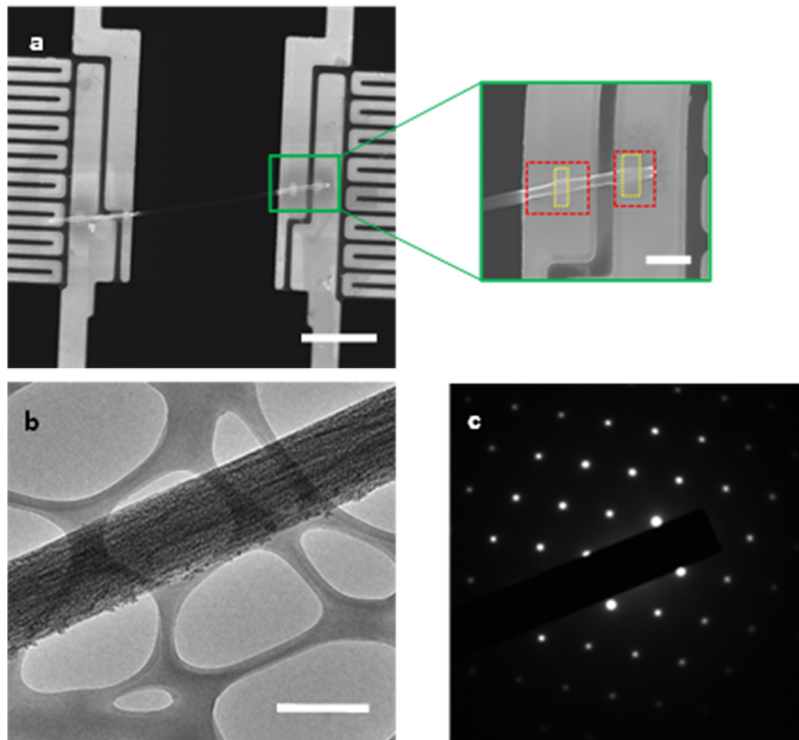

Figure S6. (a) The porous silicon nanowire on the METS device. The red dashed squares and yellow dashed squared in the inset are the ion beam etched area and the platinum deposition area; (b) An Al-doped porous silicon nanowires on holey-carbon TEM grid; (c) Diffraction pattern of nanowire in (b). The scale bars for the device and the inset are 5μm and 2μm, respectively. The scale bar for (b) is 300nm.

S5. Raman scattering measurements on individual porous nanowire

Raman scattering using a WITEC alpha 300 system was employed in order to study the optical phonons of porous silicon nanowires. A constant power <0.25mW was employed to eliminate any local heating induced Raman peak shift[14]. 3- and 4- order Si-O rings appear largely in vitreous SiO_2 due to the minimum surface energy, which have a typical Raman peak at 490 cm^{-1} and 606cm^{-1}, respectively[15, 16]. Further, as shown in Figure S7, the first order Raman peak of 514.65 cm^{-1} was shifted from bulk silicon (520cm^{-1}), possibly due to phonon confinement. The sub-peak at 490.32 cm^{-1} appeared in the as-grown porous silicon nanowires and it is present as well for the nanowires that were placed in air for a few hours, indicating that this peak is not due to additional oxide formation. We did not find the appearance of 4-order Si-O rings in our porous silicon nanowire, possibly due to the low concentration (less than 1%) of planar rings[15]. We hypothesize that the presence of this additional Raman peak at 490.32 cm^{-1} indicates that the silicon atoms closest to the surface do not form harmonic bonds with neighbouring silicon atoms, instead forming anharmonic bonds with the oxygen. This could indicate local strain near the surface, resulting in softening of phonon modes and an additional mechanism to reduce phonon transport further. For such large surface-to-volume ratio samples, the possible effect of anharmonic surface bonds has not been considered experimentally before, although it has been theoretically predicted that the oxygen vibrational spectra would overlap with silicon at some frequencies and result in a further reduction of thermal conductivity[17].
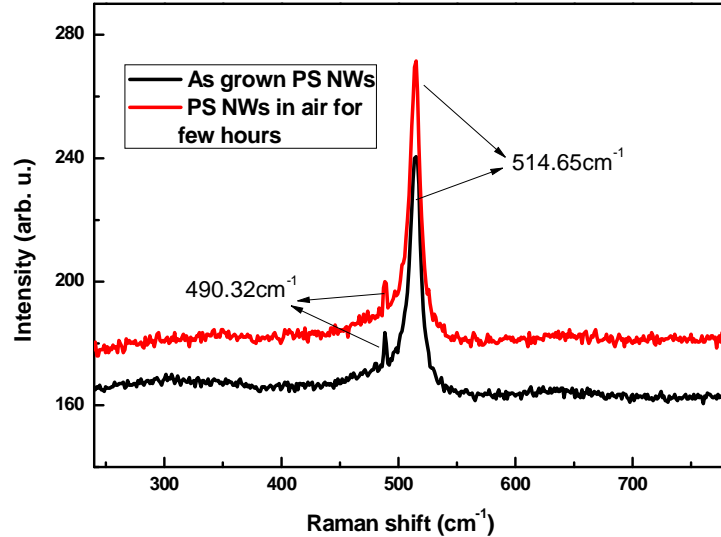
Figure S7. Black curve is the Raman spectrum of a porous silicon nanowire after growth. The red curve is for a porous silicon nanowire placed in air for a few hours. The peaks at 490.32cm^{-1} and 514.65cm^{-1} are for 3-order Si-O rings and TO Silicon modes respectively.

S6. Measurement of Young's modulus of porous silicon nanowires

Young's modulus of porous silicon nanowires is estimated from three-point bending test[18, 19] conducted on a total of twelve samples with high and low porosity. Each nanowire was placed over a 5 μm hole fabricated by Focused Ion Beam (FIB) milling and secured at both ends with Pt deposition Figure S8 (c) shows this representative 3D height image of a suspended NW and inset is its 2D image. The experiments were performed using a Dimension Icon AFM (Bruker). Force curves were obtained using the Peak Force Quantitative Nanomechanical Mapping (QNM) mode of the AFM. A cantilever (OTR8, Bruker) with a nominal spring constant of 0.57 N/m was used. The maximum force was kept below 50nN to ensure the NW undergoes elastic bending. The AFM probe oscillated

at a frequency of 2 kHz and peak-to-peak amplitude in air of 300nm. A scan rate of 0.4Hz was used. This allows 256*256 force curves to be captured over an area of about 10*10 μm². A typical force curve is shown in Figure S8 (d). The data was processed using Bruker Nanoscope Analysis 1.70 software. The largest measured deflection was used for calculation of the Young's modulus, which corresponds to the midspan of the measured nanowire. The method for extracting the vertical deflection is detailed elsewhere[20]. The simple beam theory for a cantilever beam fixed at both ends was used to obtain the Young's modulus of a NW with circular cross-section. It is given by[19, 21]

$$E = \frac{FL^3}{192I\delta}$$

where E is the Young's modulus, F is the loaded force, L is the suspended length of the nanowire, I is the moment of inertia and δ is the vertical deflection at the midspan of the nanowire. Typically, for a circular solid cross-section $I = \frac{\pi D^4}{16}$, where D is the diameter of the nanowire. Considering the porosity of silicon nanowires, the moment of inertia is different in comparison with the solid structures[22] and further mathematical calculation is carried out as follows.

As shown in the polar coordinate image of Figure S9 (a), the second moment of area, I_x, for solid silicon nanowire with a diameter of D is calculated as

$$I_{x,solid} = \iint_R y^2 \, dA_{solid} = \iint_R (rsin\theta)^2 dA_{solid} = \int_0^{2\pi} \int_0^{\frac{D}{2}} (rsin\theta)^2 \, (rdrd\theta)$$

$$= \int_0^{2\pi} \int_0^{\frac{D}{2}} r^3 \, sin^2\theta drd\theta = \int_0^{\frac{D}{2}} \frac{D^4 sin^2\theta}{64} d\theta = \frac{\pi D^4}{64}$$

Similarly, the second moment of area, I_y, is obtained to be the same value of $\frac{\pi D^4}{64}$.

For porous silicon nanowire with a cross section akin to Figure S9 (b), the per-increment in the second moment of area is

$$dI_{x,porous,1} = y^2 dA_{porous,1} = (r\sin\theta)^2 dA_{porous,1} = (r\sin\theta)^2((1 - P_1)rdrd\theta))$$

where P_1 is the porosity in the per-area of $dA_{porous,1}$, considering the non-uniformity of pores distribution along the axial direction at the integral element of dr.

Similarly, we get

$$dI_{x,porous,2} = y^2 dA_{porous,2} = (r\sin\theta)^2 dA_{porous,2} = (r\sin\theta)^2((1 - P_2)rdrd\theta))$$

$$dI_{x,porous,3} = y^2 dA_{porous,3} = (r\sin\theta)^2 dA_{porous,3} = (r\sin\theta)^2((1 - P_3)rdrd\theta))$$

$$.........$$

$$dI_{x,porous,N} = y^2 dA_{porous,N} = (r\sin\theta)^2 dA_{porous,N} = (r\sin\theta)^2((1 - P_N)rdrd\theta))$$

Therefore, $I_{x,porous} = dI_{x,porous,1} + dI_{x,porous,2} + dI_{x,porous,3} + \cdots + dI_{x,porous,N}$

$$= \int_0^{2\pi} \int_0^{\frac{D}{2}} (r\sin\theta)^2 \left(\left(\frac{1 - P_1 + 1 - P_2 + 1 - P_3 + \cdots + 1 - P_N}{N} \right) rdrd\theta \right)$$

$$= \int_0^{2\pi} \int_0^{\frac{D}{2}} (r\sin\theta)^2 ((1 - P)rdrd\theta) = (1 - P)\frac{\pi D^4}{64}$$

where P is the average porosity along the nanowire.

And, $I_{y,porous} = (1 - P)\frac{\pi D^4}{64}$.

For the Young's modulus calculation of porous silicon nanowires, this effective moment of inertia caused by porosity effect is used.
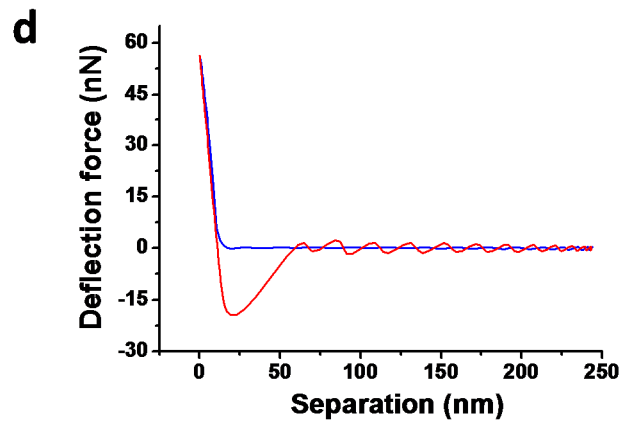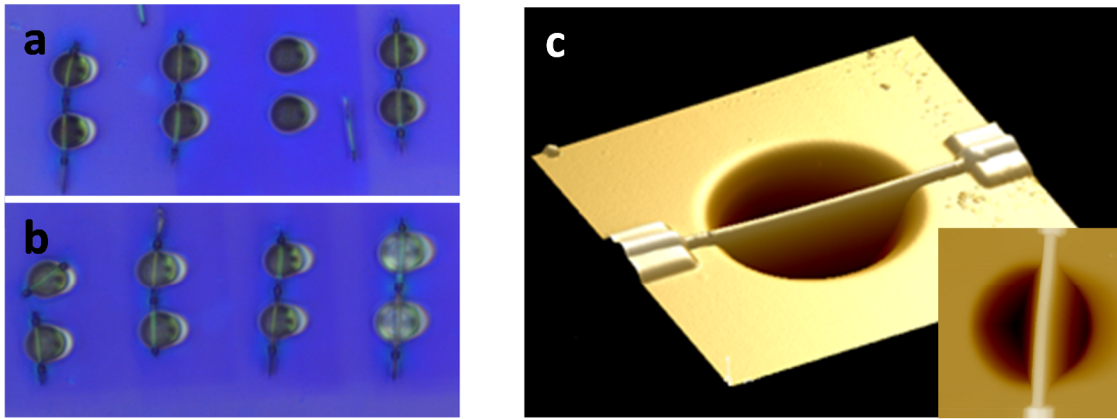
Figure S8. (a)-(b) Optical images of the measurement setup. The holes are etched on a Silicon substrate using a Focused Ion Beam (FIB). The nanowires are placed over the holes by nano-manipulator in SEM and the ends are fixed by Electron Beam Induced platinum Deposition (EBID). (c) 3-D image of measured nanowire under AFM contact mode. Inset is the corresponding 2-D top-view image. (d) The typical deflected separation vs force at the mid-point of the nanowire used to calculate the Young's modulus.
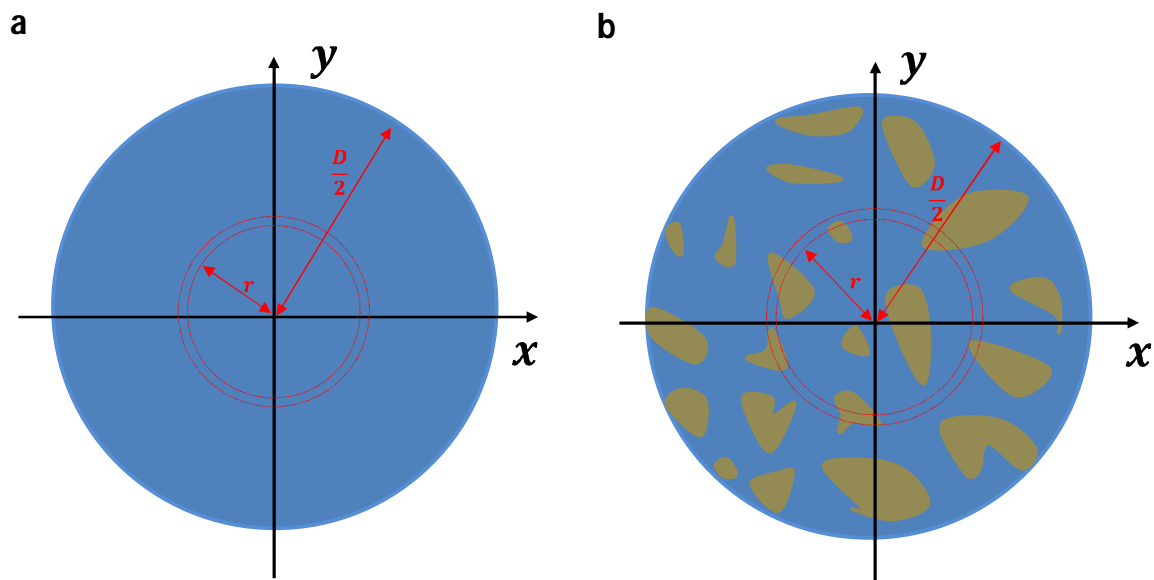
Figure S9. Schematic of a circular cross-section silicon nanowire solid (a) and porous (b) silicon nanowires.

D is the diameter and r is the radius used in the integral.

S7. Molecular dynamics (MD) simulation

<u>Thermal conductivity simulation:</u>

Nonequilibrium molecular dynamics (NEMD) is employed to calculate the thermal conductivity of pure silicon and nanoporous silicon nanowires. The software LAMMPS[23, 24] is used to perform the NEMD calculation. Free boundary condition is set at the surface of porous Si nanowire and the fixed boundary condition is set in the longitudinal direction. We use the Stillinger-Weber (SW)[25] potential for Si, which includes both two-body and three-body potential terms. The SW potential has been used widely to study the thermal properties of Si structures[26, 27]. A temperature gradient is

established along the longitudinal direction by applying Langevin heat bath at the two ends.

The equations of motions are integrated by velocity Verlet method with a time step of 0.8 fs. In the beginning, the simulation runs 3.2 ns to reach a steady state by applying heat bath at the two ends. Then the simulation runs 11.2 ns to get an averaged heat current and temperature profile. The thermal conductivity is calculated from Fourier's law

$$\kappa = -\frac{J \cdot L}{A \cdot \Delta T}$$

S (7)

where J is the heat current, L is the length of the simulation cell, ΔT is the temperature difference and A is the cross section area. In our simulation, the two heat baths with temperatures of T_L=310 K and T_R=290 K are applied at left and right ends, respectively. There are temperature jumps at the two boundaries due to coupling with the heat baths. ΔT is defined as the temperature difference between the two dashed lines, which excludes the temperature jumps next to heat bath. The thermal conductivity is averaged over six simulations with different initial conditions. The error bar is the standard deviation of the six simulation results. Figure S10 shows the structure of pure and porous silicon nanowires with different porosity: (a), (c), (e), (g), (i) and (k) are silicon nanowires before relaxing; (b),(d), (f), (h), (j) and (l) are after relaxing. Table S3 summarizes simulation results for porous silicon nanowires with different porosity.

Young's modulus simulation:

The Young's modulus of Silicon Nanowires is also calculated by molecular dynamics at 300 K. In classical mechanics, the Young's modulus is defined as $Y = \frac{\sigma}{\varepsilon} = \frac{\sigma}{\Delta L/L_0}$,

where σ is the axial stress, ε is the strain, L_0 is the initial length and ΔL is the elongation under the stress σ. A Langevin heat bath is applied to equilibrate the system at 300 K by running 20,000 steps. In addition, molecular dynamics run another 6,000 steps to obtain the stress for the system with length L_0 and $L_0+\Delta L$, respectively. Finally, Young's modulus is calculated by averaging six simulations with different initial conditions, and the error bar is the standard deviation of the six simulations. The Young's modulus of bulk Si at 300 K and 0 K are calculated as 150.6 ±0.54 and 151.4 GPa, respectively, which is the same as the analytical result by Cowley at zero K[28]. The Young's modulus of crystalline SiNW with 8 nm diameter cross section and 50 nm length is 68.7 GPa and 65.3 GPa for non-passivated and oxygen passivated crystalline SiNW, respectively. With increasing porosity, the Young's modulus of porous nanowires decreases and all the data are summarized in Figure S11.
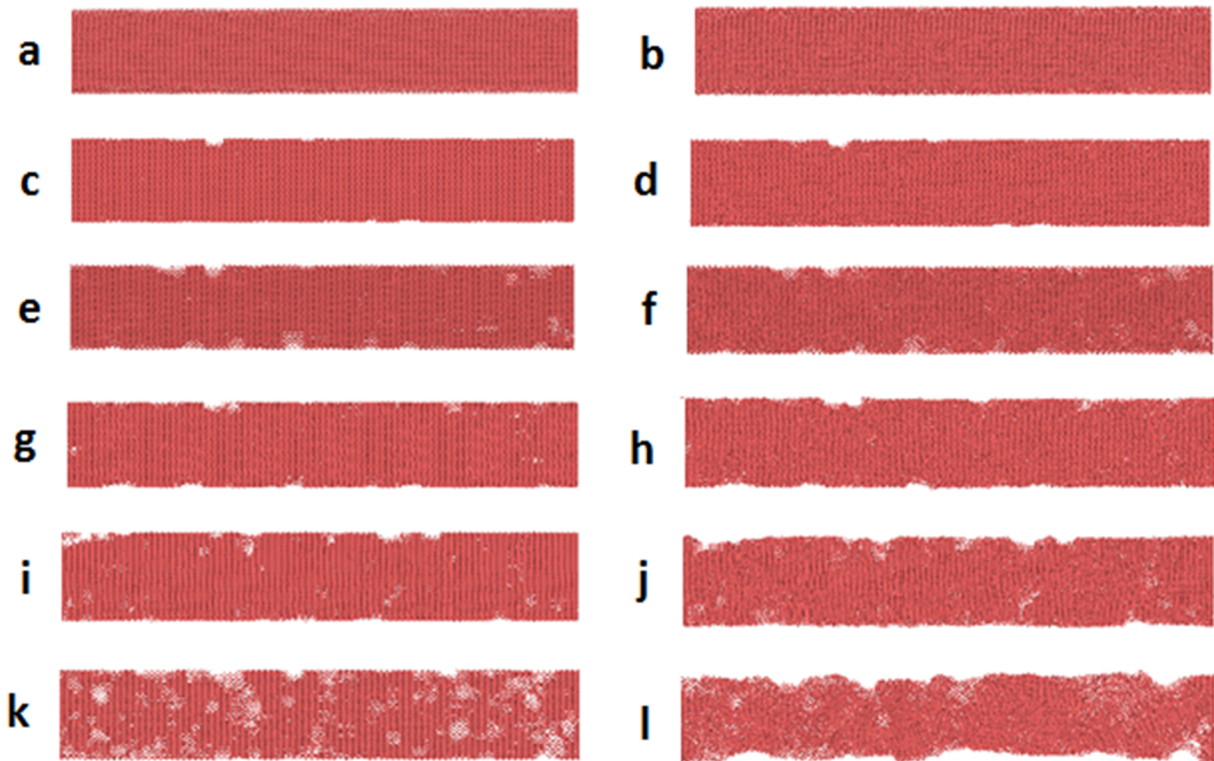
Figure S10. Pure silicon nanowire and porous silicon nanowires with different porosity before and after relaxation. (a), (c), (e), (g), (i) and (k) are silicon nanowires before relaxation. (b), (d), (f), (h), (j) and (l) are silicon nanowires with the same porosity, respectively, after relaxation. (a), (b) are pure silicon and (c)-(l) are porous silicon. Porosity for (c), (e), (g), (i) and (k) is 5%, 10%, 22%, 32% and 43%, respectively.
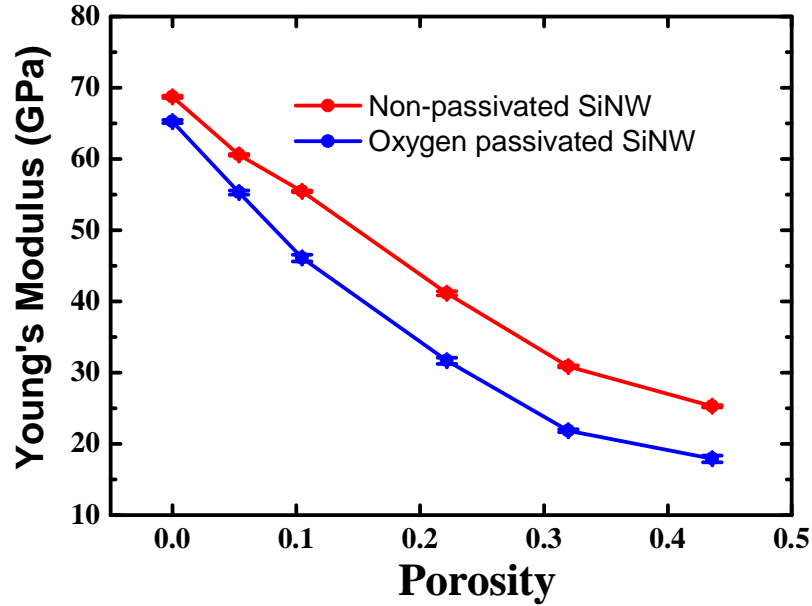

Figure S11. Young's modulus of non-passivated SiNW and Oxygen passivated SiNW calculated using molecular dynamics simulations at 300 K. The length and the diameter of cross section of SiNW is 50 nm and 8 nm respectively. The Young's modulus decreases as porosity increases and Oxygen passivation decreases the Young's modulus further, in line with real samples.

Table S3. MD simulation for the thermal conductivity of porous silicon nanowires with different porosity

Porosity	Thermal conductivity (W/m-K)	Error bar (W/m-K)
5.37%	8.70	0.15
10.47%	5.10	0.052
22.15%	2.02	0.056
31.97%	1.13	0.047
43.59%	0.77	0.032

S8. Phonon dispersion calculation for Si nanowires

To better show how phonons behave in the nanostructures with a reduced size down to few nanometers, we carry out simulations to calculate the phonon dispersion. This was done using the General Utility Lattice Program (GULP)[29]. We calculate the phonon dispersion of three structures (a) bulk Silicon (Si), (b) Si nanowire (SiNW) with 5.4 nm diameter and (c) SiNW with 4.3nm diameter. Here we use one conventional cell in the longitudinal direction for all the three cases. In the transverse direction, the 5.4 nm SiNW has ten unit cells and the 4.3 nm diameter SiNW has eight unit cells. The wave vectors are normalized to one. As shown in Figure S12, the phonon dispersions of Si nanowire with a small diameter (similar to our structure size) are different compared with those of bulk Si. The acoustic phonon modes of SiNW with 4.3 nm diameter are similar to those of the 5.4 nm diameter SiNW, but their group velocities are decreased compared with that of bulk Si, which indicates that these phonon modes are softened. The optical phonon modes of Si nanowire from 0.5 THz to the highest frequency are all affected compared with bulk Si, although these are short mean free path phonons that carry smaller

percentage of the heat. The thermal conductivity is mostly determined by the acoustic phonon modes.
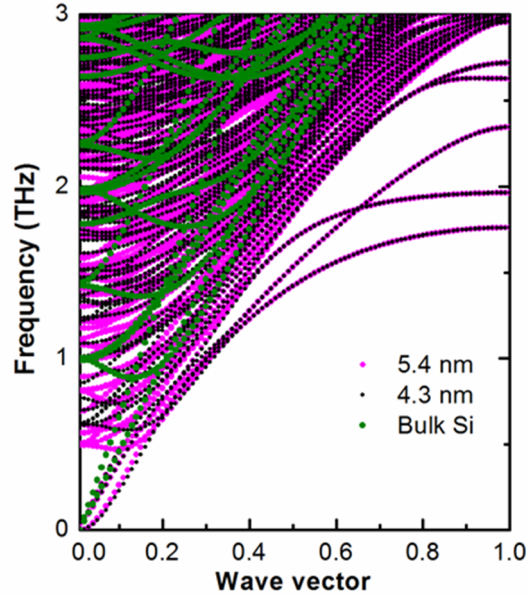

Figure S12. Phonon dispersion of Si nanowire along the longitudinal direction. Phonon dispersion of bulk Si is shown for comparison. The pink, black and green dots are the phonon modes of Si nanowire with diameter 5.4 nm, 4.3 nm and bulk Si, respectively.

S9. Specific heat for porous silicon nanowires

To verify the hypothesis that the specific heat of porous silicon nanowires is similar with that of bulk silicon, we re-calculate the specific heat based on our experimental values of thermal conductivity, $\kappa(T, d)$. That is,

$$C_{calc,porous}(T) = \frac{3 \cdot \kappa(T,d)}{v \cdot (\frac{1}{r_{bulk}(T)} + \frac{4}{3d})^{-1}},$$

Here, v is the average phonon group velocity estimated based on Figure 4(d), $r_{bulk}(T)$ is the bulk phonon mean free path as originally obtained in the manuscript and d is the structure size of the

measured porous nanowires. This calculated specific heat is shown as blue stars in Figure S13. It shows that the specific heat for porous silicon nanowires with structural size of 4-5nm is comparable with the bulk silicon specific heat in the measured temperature regime.
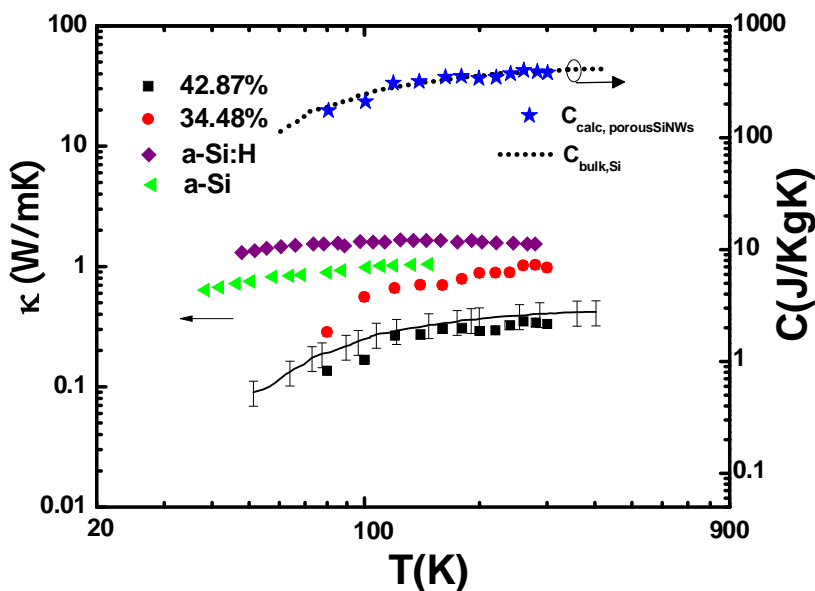

Figure S13. Temperature-dependent thermal conductivity of porous silicon nanowire together with a-Si (green triangles) and a-Si:H (purple diamonds). On the right side is the temperature dependent specific heat for bulk silicon and the blue stars are the calculated specific heat for porous silicon nanowires. The black solid lines are fitted from the EPRT model.

On the other hand, the effect of phonon confinement on the specific heat has been discussed for the case of silicon nanowires by solving the elastic wave equation[30]. They calculated the specific heat for silicon nanowires with small diameters down to 2.7 nm and it turns out that the effect of phonon confinement on specific heat becomes significant at temperatures below 30K for a silicon nanowire with a diameter of 2.7 nm, a structure size smaller than those we've measured in our study. With increasing temperature, the specific heat of silicon

nanowire is similar to bulk and the transition temperature from 1D to 3D for the 10.8nm diameter silicon nanowire is ~20K.

References

[1]   X. Li, P. Bohn, *Appl. Phys. Lett.* **2000**, 77, 2572.

[2]   Z. Huang, X. Zhang, M. Reiche, L. Liu, W. Lee, T. Shimizu, S. Senz, U. Gösele, *Nano Lett.* **2008**, 8, 3046.

[3]   J. Tang, H.-T. Wang, D. H. Lee, M. Fardy, Z. Huo, T. P. Russell, P. Yang, *Nano Lett.* **2010**, 10, 4279.

[4]   V. Lysenko, S. Perichon, B. Remaki, D. Barbier, B. Champagnon, *J. Appl. Phys.* **1999**, 86, 6841.

[5]   B. Kim, J. Nguyen, P. J. Clews, C. M. Reinke, D. Goettler, Z. C. Leseman, I. El-Kady, R. H. Olsson, in *Proc. IEEE 25th Int. Conf. Micro Electro Mech. Syst. (MEMS),* **2012**, doi: 10.1109/MEMSYS.2012.6170122.

[6]   J.-K. Yu, S. Mitrovic, D. Tham, J. Varghese, J. R. Heath, *Nat. Nanotechnol.* **2010**, 5, 718.

[7]   J. Goldstein, D. Newbury, D. Joy, C. Lyman, P. Echlin, E. Lifshin, L. Sawyer, J. Michael, *Scanning Electron Microscopy and X-ray Microanalysis,* Kluwer Academic, Plenum Publishers, New Youk (USA) **2003**, p. 688.

[8]   H. Bethe, *Ann. Phys.* **1930**, 397, 325.

[9]   D. Joy, S. Luo, *Scanning* **1989**, 11, 176.

[10]   K. Kanaya, S. Okayama, *J. Phys. D Appl. Phys.* **1972**, 5, 43.

[11]   M. Rauer, M. Rüdiger, C. Schmiga, H. Strutzberg, M. Bähr, M. Glatthaar, S. W. Glunz, *J. Appl. Phys.* **2013**, 114, 203702.

[12]   A. I. Hochbaum, R. Chen, R. D. Delgado, W. Liang, E. C. Garnett, M. Najarian, A. Majumdar, P. Yang, *Nature* **2008**, 451, 163.

[13]   A. Colli, A. Fasoli, C. Ronning, S. Pisana, S. Piscanec, A. C. Ferrari, *Nano Lett.* **2008**, 8, 2188.

[14]   S. Piscanec, M. Cantoro, A. Ferrari, J. Zapien, Y. Lifshitz, S. Lee, S. Hofmann, J. Robertson, *Phys. Rev. B* **2003**, 68, 241312.

[15]   F. Galeener, *Solid State Commun.* **1982**, 44, 1037.

[16]   A. L. Linsebigler, G. Lu, J. T. Yates Jr, *Chem. Rev.* **1995**, 95, 735.

[17]   J. Fang, L. Pilon, *Appl. Phys. Lett.* **2012**, 101, 011909.

[18]   B. Varghese, Y. Zhang, L. Dai, V. B. Tan, C. T. Lim, C.-H. Sow, *Nano Lett.* **2008**, 8, 3226.

[19]   H. Ni, X. Li, H. Gao, *Appl. Phys. Lett.* **2006**, 88, 043108.

[20]   E. Tan, C. Lim, *Appl. Phys. Lett.* **2004**, 84, 1603.

[21]   B. Wu, A. Heidelberg, J. J. Boland, *Nat. Mater.* **2005**, 4, 525.

[22]   D. Choi, J. Jeon, P. Lee, W. Hwang, K. Lee, H. Park, *Compos. Struct.* **2007**, 79, 548.

[23]   V. Varshney, A. K. Roy, G. Froudakis, B. L. Farmer, *Nanoscale* **2011**, 3, 3679.

[24]   Y. Lee, S. Lee, G. S. Hwang, *Phys. Rev. B* **2011**, 83, 125202.

[25]   F. H. Stillinger, T. A. Weber, *Phys. Rev. B* **1985**, 31, 5262.

[26]   N. Yang, G. Zhang, B. Li, *Nano Lett.* **2008**, 8, 276.
[27]   A. S. Henry, G. Chen, *J. Comput. Theor. Nanosci.* **2008**, 5, 141.
[28]   E. R. Cowley, *Phys. Rev. Lett.* **1988**, 60, 2379.
[29]   J. D. Gale, *J. Chem. Soc. Faraday Trans.* **1997**, 93, 629.
[30]   R. Prasher, T. Tong, A. Majumdar, *Nano Lett.* **2008**, 8, 99.